RESEARCH ARTICLE

Cage-size effects on the encapsulation of P_2 by fullerenes

Enric Sabater[1,2] 🆔 | Miquel Solà[2] 🆔 | Pedro Salvador[2] | Diego M. Andrada[1] 🆔

[1]Department of Chemistry, Faculty of Natural Sciences and Technology, Saarland University, Saarbrücken, Germany

[2]Institut de Química Computacional i Catàlisi and Departament de Química, Universitat de Girona, Girona

Correspondence

Diego M. Andrada, Department of Chemistry, Faculty of Natural Sciences and Technology, Saarland University, 66123, Saarbrücken, Germany.
Email: diego.andrada@uni-saarland.de

Pedro Salvador, Institut de Química Computacional i Catàlisi and Departament de Química, Universitat de Girona, C/ M. Aurèlia Capmany 69, 17003, Girona.
Email: pedro.salvador@udg.edu

Abstract

The classic pnictogen dichotomy stands for the great contrast between triply bonding very stable N_2 molecules and its heavier congeners, which appear as dimers or oligomers. A banner example involves phosphorus as it occurs in nature as P_4 instead of P_2, given its weak π-bonds or strong σ-bonds. The P_2 synthetic value has brought Lewis bases and metal coordination stabilization strategies. Herein, we discuss the unrealized encapsulation alternative using the well-known fullerenes' capability to form endohedral and stabilize otherwise unstable molecules. We chose the most stable fullerene structures from C_n (n = 50, 60, 70, 80) and experimentally relevant from C_n (n = 90 and 100) to computationally study the thermodynamics and the geometrical consequences of encapsulating P_2 inside the fullerene cages. Given the size differences between P_2 and P_4, we show that the fullerenes C_{70}–C_{100} are suitable cages to side exclude P_4 and host only one molecule of P_2 with an intact triple bond. The thermodynamic analysis indicates that the process is favorable, overcoming the dimerization energy. Additionally, we have evaluated the host-guest interaction to explain the origins of their stability using energy decomposition analysis.

KEYWORDS
bonding analysis, encapsulation, endohedral, energy decomposition analysis, multiple bond

1 | INTRODUCTION

Stable compounds featuring multiple bonds between heavy main group elements have long been thought unrealizable.[1] Consequently, the so-called "double-bond rule" emerged, formalizing the impossibility of achieving them due to the relative weakness of π-bonds of those p-block elements beyond the second period, providing fundamental instability of compounds.[2] Eventually, this rule was disproven by synthetic strategies based on sterically crowded substituents and coordination to Lewis bases/acid pairs to provide kinetic and thermodynamic stability.[3] Thus, experimental achievement recounts compounds containing double and triple bonds between Groups 13, 14, and 15 tricoordinate and dicoordinate atoms.[4]

The unsaturated Group 15 compounds belong to a captivating chapter of this topic with the classic pnictogen dichotomy.[5] Although triply bonded diatomic N_2 species is a ubiquitous inert gas,[6] its heavier homologues are highly reactive and prone to form oligomers. For instance, the most stable phosphorus species is tetra-atomic P_4 (T_d) white phosphorus,[7] whereas P_2 is only found as free molecules at high temperatures in the gas phase[8] or in isolation matrices at 17 K.[9] The dimerization process from P_2 to form P_4 has been experimentally estimated to be thermodynamically favorable by 53.6 kcal/mol.[10] This observation has been traditionally explained according to the double
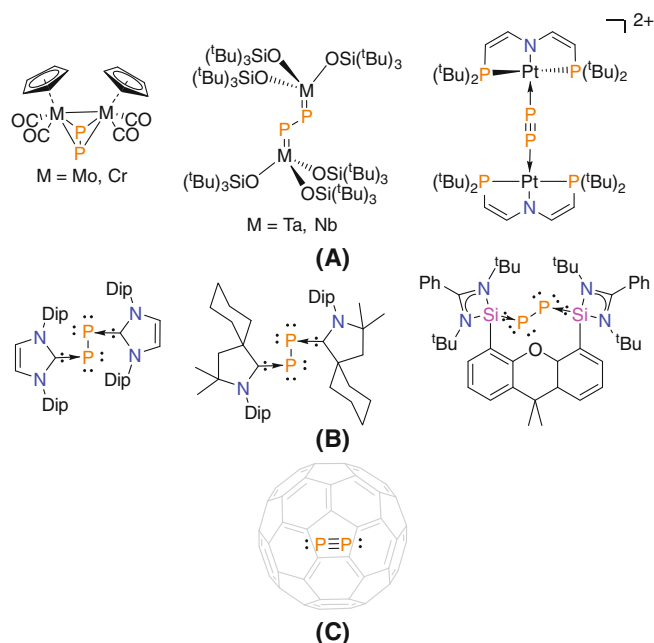
SCHEME 1 Stabilization approaches of P_2 triple bond unit: (A) transition metal coordination; (B) Lewis base stabilization; (C) encapsulation approach. Dip = 2,6-diisopropyl-phenyl; ^tBu = *tert*-butyl.

bond rule, suggesting a weak π-bond between the phosphorus atoms.[11] In contrast, Kutzelnigg discussed that taking into account only the overlap populations, it is expected that the triple bond in N_2 and P_2 are approximately equal in strength.[12] However, he pointed out that the bond strength also depends on how strongly the valence electrons are attached to the elements, and hence, in qualitative terms, the bond energy on N_2 is significantly stronger than P_2.[12] Many years later, Jerabek and Frenking brought a quantitative assessment using energy decomposition analysis (EDA).[13] Notably, they found that the contribution of the π-bonding in P_2 (40.5%) is higher than in N_2 (34.4%). Thus, the tendency of P_2 to dimerize is related to the enhanced stability due to the σ-bonds formed rather than π-bonding lost.

The constant quest for environmentally friendly processes which are of preparative value has triggered many investigations on the introduction of phosphorus atoms under mild conditions.[14] In this vein, P_2 is an interesting reagent for producing heterocycles via cycloadditions, for instance.[15] However, its use in synthesis requires the stabilization preserving the triply bonded P≡P moiety. Strategies based on transition-metal mediated degradation of the P_4 into P_2 units have been extensively explored in the past (Scheme 1A).[16] The outcome of these reactions is a side-on bridging M_2P_2 coordination mode, yielding a significant decrease in the multiple bond character relative to free P_2.[17] Nonetheless, a landmark study by Cummins and co-workers demonstrated that niobium-based coordination can be used for the thermal transfer of P_2 to 1,3-dienes.[18] End-on M≡P—P≡M coordination modes are rare cases, and the formation is ascribed to the steric hindrance between the metal moieties.[19] The center moiety has been described as a P—P single bond given the redox activity of the

metals.[20] Recently, Schneider, Holthausen, and co-workers reported the use of redox inactive platinum ligands as an unprecedented platform for the stabilization of P_2 as a neutral, triply bonded unit.[21] Furthermore, the stabilization by strong σ-donor Lewis bases has been also evaluated, counting N-heterocyclic carbene (NHC),[22] cyclic(alkyl)amino carbene (CAAC),[23] and the boryl,[24] and silylene analogues (Scheme 1B).[25] Similarly, the loss of the multiple bond character is observed as a result of a strong donor-acceptor interaction between the Lewis base lone pair and the π* orbitals of the P_2 species.[26]

Strategies based on transition-metal and Lewis bases coordination have been long-standing within the P_2 feedstock methods. There is, however, an unrealized alternative based on the size change from P_2 to P_4 species. In this sense, one could envisage an approach using the ability of fullerenes to encapsulate and form stable endohedral complexes with atoms and small molecules.[27] The chemistry of endohedral started directly after the seminal discovery of fullerenes with the characterization of La@C_{60}.[28] Six years later, endohedral fullerenes (EF) with encapsulated noble gases were synthesized by collision of helium, neon or argon atoms with C_{60}^+ or of noble gas cations with neutral C_{60}.[29] Since then, a plethora of endohedral fullerenes–as well as several synthetic derivatives–have been reported. Classical EFs are those of the type M@C_n, M_2@C_n, and M_3@C_n (M = Li, Ca, Pr, Y, Ba, Ce, Nd, and Gd, among others or noble gases and 60 < n < 88).[30] On the other hand, EFs that involve metal clusters are called endohedral metallofullerenes (EMFs).[27] Among them, we can distinguish between the following types[31]: (i) metallic nitride EMFs (M_3N@C_n, M = metal and 68 < n < 96); (ii) metallic carbide EMFs (M_2C_2@C_n, M_3C_2@C_n, M_4C_2@C_n, and M_3CH@C_n with M = metal and 68 < n < 92); (iii) metallic oxide EMFs (M_4O_2@C_n and M_4O_3@C_n); (iv) metallic sulfide EMFs (M_2S@C_n); and (v) dimetallic EMFs (M_2@C_n). The most well-known EMF is Sc_3N@I_h-C_{80} that is the third most abundant fullerene after C_{60} and C_{70}.[32] Finally, another group of EFs contain small molecules such as H_2,[33] H_2O,[34] CO,[35] HF,[36] CH_4,[37] NH_3,[38] N_2 and CO_2,[39] and O_2 and H_2O_2,[40] which are introduced in many cases with a procedure called molecular surgery.[41] With this procedure, Murata et al. have also introduced H_2 into C_{70}, observing a relative population of 97:3 of H_2@C_{70} and $2H_2$@C_{70}.[42]

It is known that there must be enough space inside the fullerene cage to encapsulate an atom, a cluster, or a molecule. Otherwise, the interaction between the encapsulated atom (molecule) and the fullerene cage becomes energetically unfavorable.[27] Nonetheless, in some cases, the guest can also modify and define the shape of the host.[43] The reported van der Waals radii of P and sp^2 C atoms are both approximately 1.80 Å,[44] and the P_2 and P_4 bond lengths are 1.893 Å and 2.223 Å, respectively.[45] Thus a total (C··· P≡P ···C) distance of ca. 9.1 Å would be required for encapsulation of P_2, while for P_4 the distance would increase up to ca. 9.4 Å. By simple geometrical considerations, a size exclusion effect could be feasible by fullerenes between C_{70} (cage diameter 8.33 Å) and C_{90} (cage diameter 10.74 Å). However, whether the encapsulation stabilization would be sufficient to overcome the thermodynamic challenge of P_2 dimerization needs to be evaluated. This systematic

study aims to give a comprehensive overview of the structural and electronic features of endohedral fullerenes C_n (n = 50, 60, 70, 80, 90, and 100) upon encapsulation of P_2, and also the evaluation of the dominating physicochemical factors.

2 | METHODS

All structures were optimized with a combination of Turbomole 7.3.1 software[46] and Gaussian 16 C.01 software.[47] Initial fullerene geometries of a given isomer were extracted from the Fullerene software.[48] This program uses the face-spiral algorithm of Manolopoulos and Fowler with a force field optimization to generate the fullerene coordinates.[49] Geometry optimizations were performed at the BP86-D3 (BJ)/def2-SVP level of theory without symmetry constraints. Analytical harmonic frequencies were computed to determine the nature of stationary points and to calculate unscaled zero-point energies (ZPEs) as well as thermal corrections and entropic effects using the standard statistical-mechanics relationships for ideal gas.[50] Single-point BP86-D3(BJ)/def2-TZVP calculations were also performed at the stationary points to improve the electronic energies. The basis set superposition error (BSSE) has been assessed through single-point calculations with the counterpoise method.[51]

Electronic structure analyses have been performed on the BP86-D3(BJ)/def2-TZVP wavefunction. Natural Population Analysis (NPA)[52] and the associated Wiberg bond orders have been carried out using GENNBO 7.0 program.[53] The formal partial charges were obtained using the topological fuzzy Voronoi cells (TFVC) atomic definition[54] as implemented in APOST3D code.[55]

The nature of the host-guest interaction was investigated by means of the EDA, developed by Morokuma[56] and by Ziegler and Rauk,[57] at the BP86-D3(BJ)/TZ2P[58] level of theory using ADF2019.101. Core electrons were treated by the frozen-core approximation and scalar relativistic effects have been incorporated by the zeroth-order regular approximation (ZORA).[59]

The bonding analysis focuses on the instantaneous interaction energy ΔE_{int} of a bond A–B between two fragments A and B in the particular electronic reference state and in the frozen geometry AB. This energy is divided into four main components (Equation 1).

$$\Delta E_{int} = \Delta E_{elst} + \Delta E_{Pauli} + \Delta E_{orb} + \Delta E_{disp} \quad (1)$$

The term ΔE_{elst} corresponds to the quasiclassical electrostatic interaction between the unperturbed charge distributions of the prepared atoms (or fragments) and it is usually attractive. The Pauli repulsion ΔE_{Pauli} is the energy change associated with the transformation from the superposition of the unperturbed densities of the isolated fragments to the wave function $\Psi_0 = N\hat{A}[\Psi_A\Psi_B]$, which properly obeys the Pauli principle through explicit antisymmetrization ($\hat{A}$ operator) and renormalization (N = constant) of the product wave function. It comprises the destabilizing interactions between electrons of the same spin on either fragment. The orbital interaction ΔE_{orb} accounts for bond pair formation, charge transfer, and polarization effects from the intermediate state to the final AB wavefunction.[60] In the case

dispersion corrections[51b,61] are introduced, the term ΔE_{disp} is computed and added to Equation 1. Further details on the EDA method can be found in the literature.[62] In the case of the dimers, relaxation of the fragments to their equilibrium geometries at the electronic ground state is termed ΔE_{prep}, because it may be considered as preparation energy for chemical bonding. The addition of ΔE_{prep} to the intrinsic interaction energy ΔE_{int} gives the total energy ΔE, which is, by definition, the opposite sign of the bond dissociation energy D_e, in this case associated to the encapsulation energy:

$$\Delta E(-D_e) = \Delta E_{int} + \Delta E_{prep} \quad (2)$$

3 | RESULTS AND DISCUSSION

3.1 | Geometries and energetics

The most stable isomer of C_{60} is the well-known $C_{60}-I_h$(#1812), the only C_{60} isomer obeying the isolated pentagon rule (IPR).[63] Similarly, for C_{70} the experimentally characterized isomer is the $C_{70}-D_{5h}$ (#8149) one.[64] There is no IPR structure for C_{50} and previous computational studies point to the $C_{50}-D_{5h}$(#271) and $C_{50}-D_3$(#270) isomers as the most stable ones,[65] depending on the particular level of theory applied. For C_{80}, the experimentally characterized isomer is the $C_{80}-D_2$(#31919).[66] Sure et al. computational studied all 31,924 isomers of C_{80} and found several additional isomers close in energy.[67] In particular, isomer $C_{80}-D_{5d}$(#31918) was found the most stable one at PBE-D3/def2-TZVP level of theory, while $C_{80}-D_2$(#31919) was found the lowest energy isomer for DLPNO-CCSD(T)/CBS energies. Finally, Koenig et al. have recently experimentally characterized tubular $C_{90}-D_{5h}$ and $C_{100}-D_{5d}$ isomers.[68]

It is worth noting that for C_{80}, the cage of I_h symmetry is the most unstable among the seven isomers of C_{80} that satisfy the IPR.[69] However, this cage leads to the most favored EMFs when two La atoms or a Sc_3N unit are present inside $C_{80}-I_h$. This result shows that the relative stability of the different cages can change when atoms or metallic clusters are encapsulated inside the cage. However, as we will show later, interaction of P_2 with the cage is relatively weak, and, therefore we do not expect major changes in the stability of the cages due to P_2 encapsulation. Moreover, the determination of the global minima of all $P_2@C_n$, n = 50, 60, 70, 80, 90, and 100 is out of the scope of this work. In addition to the particular C_n isomer, one has to take into account that the P_2 moiety can exhibit different orientations inside the cage. For this reason, we have performed an exploratory study of the $P_2@C_{60}$ species. Thus, we have considered first the $C_{60}-I_h$ isomer and up to four different well-defined orientations of the P_2 unit inside the cage (see Table S3). Note that the encapsulation of P_2 lowers the symmetry of the pristine cage, depending on its specific position inside. In the D_{5d} geometry, the internuclear P–P bond axis is collinear with the center of opposing pentagon poles. Similarly, a C_{3v} symmetry is achieved by placing the P–P bond collinear with the center of opposing six-membered rings (6-MRs). The third and the fourth structures were considered where the P–P bond axis is collinear with the midpoints of two opposing 6,6- and 5,6-type C–C bonds, with

TABLE 1 Relative energies (in kcal/mol) of selected C_n isomers for pristine cages and upon P_2 encapsulation. The numbering of the isomers stems from lexicographically ordered face-spiral pentagon indices. The column Symm. Refers to the change of symmetry due to encapsulation.[a]

| | Isomer | C_n | | $P_2@C_n$ | |
		Symm.	ΔE	Symm.	ΔE
C_{50}	271	D_{5h}	3.6	$D_{5h} \rightarrow C_{2v}$	0.0
	270	D_3	0.0	$D_3 \rightarrow C_3$	8.1
C_{60}	1812	I_h	0.0	$I_h \rightarrow D_{5d}$	0.0
	1809	C_{2v}	36.5	$C_{2v} \rightarrow C_{2v}$	27.2
	1804	D_3	54.4	$D_3 \rightarrow D_3$	60.7
C_{80}	31,919	D_2	0.6	$D_2 \rightarrow D_2$	0.0
	31,918	D_{5d}	2.8	$D_{5d} \rightarrow D_{5d}$	1.2
	31,920	C_{2v}	0.0	$C_{2v} \rightarrow C_{2v}$	0.5
	31,922	C_{2v}	5.0	$C_{2v} \rightarrow C_{2v}$	6.9
	31,923	D_{5h}	5.7	$D_{5h} \rightarrow D_2$	9.8

[a]All calculations performed at the BP86-D3(BJ)/def2-TZVP//BP86-D3(BJ)/def2-SVP level of theory.

symmetries D_{2h} and C_{2h}, respectively (see Figures S1-2). Both the D_{5d} and C_{2h} structures correspond to local minima, while D_{2h} and C_{3v} correspond to first- and second-order saddle points at the current level of theory. All stationary points are almost degenerated (i.e., within 0.3 kcal/mol), which would indicate that the host-guest interaction is not directional and essentially the P_2 moiety exhibits free rotation inside the cage.

Next, we have considered the P_2 encapsulation into two additional C_{60} cage isomers, namely the $C_{60}-C_{2v}$(#1809) and $C_{60}-D_3$(#1804). As shown in Table 1, relative energies with respect to the lowest energy $C_{60}-I_h$ isomer are 36.5 and 54.4 kcal/mol for the pristine cages and 27.2 and 60.7 kcal/mol for the respective P_2 endohedral species. The values for the pristine cages are in good agreement with those reported by Sure et al.[67] For small fullerenes, the effect of P_2 encapsulation on the relative energies of the C_{60} isomers is not negligible. This effect can be seen in the case of C_{50}, where the (#271) isomer is lower in energy than the (#270), which is found to be lower in energy for the pristine cage. However, when considering larger fullerenes such as C_{80}, the relative energies of the isomers are barely affected by the encapsulation of P_2. Still, pristine $C_{80}-D_2$(#31919) and $C_{80}-D_{5d}$(#31918) isomers are found to be within <1 kcal/mol at the current level of theory, and upon P_2 encapsulation the lowest energy structure is $P_2@C_{80}-D_2$(#31919) by merely 0.5 kcal/mol (see Table 1).

Figure 1 depicts the final optimized geometries of all at $P_2@C_n$ and $P_4@C_n$, n = 50-100, systems, obtained the BP86-D3(BJ)/def2-SVP level of theory together with their symmetry and the P–P bond length. On the one hand, in $P_2@C_n$ the P–P bond axis is collinear with the center of pentagon poles when possible by the geometry of the cage, as described for the C_{60} cage. This leads to $P_2@C_{70}-D_{5h}$, $P_2@C_{90}-C_{5v}$ and $P_2@C_{100}-C_{5v}$ structures. In addition, only in the

larger cages (C_{90} and C_{100}) the center of mass of the P_2 unit is slightly shifted from the geometrical center of the cage. When the cage is C_{50}, the P_2 unit is almost collinear with two opposing (5,6) C–C bonds, leading to a $P_2@C_{50}-C_{2v}$ structure. Finally, in $P_2@C_{80}-D_2$, the P_2 bond axis is collinear with the center of two opposing (6,6) C–C bonds of the cage. On the other hand, $P_4@C_n$ endohedrals achieve lower symmetry levels than $P_2@C_n$. In this case, the P_4 tetrahedron edges can point towards the center of the pentagon ($P_4@C_{50}-C_s$) or the hexagon ($P_4@C_{60}-C_{3v}$). Alternatively, one of the P–P bonds matches opposing (6,6) C–C bonds furnishing $P_4@C_{70}-C_2$, $P_4@C_{80}-D_2$, and $P_4@C_{90}-C_2$. In C_{100}, the P_4 molecule is shifted from the cage center, raising the $P_4@C_{100}-C_s$.

At the current level of theory, the bond length of free P_2 and P_4 are 1.917 and 2.233 Å, respectively, in rather good agreement with the experimentally measured for P_2 (1.893 Å)[45a] and for P_4 (2.223 Å),[45b] and also previous theoretical calculations (1.911, 2.221 Å).[13]

The encapsulation of P_2 into the smaller size cages induces a shortening of P–P bond length, down to 1.823 Å in the case of C_{50}. From C_{80} and larger cages the P_2 distance remains essentially unaffected, already pointing to the absence of electronic effects (e.g. charge-transfer) from the cage.

Encapsulation energies, given by the following equation

$$\Delta E = E_{P_2@C_n} - (E_{C_n} + E_{P_2}), \tag{3}$$

$$\Delta E = E_{P_4@C_n} - (E_{C_n} + E_{P_4}), \tag{4}$$

provide a hint about the feasibility of the formation of the endohedral species.

Table 2 gathers the electronic and Gibbs energy values obtained for the species considered. A single-point counterpoise correction to estimate the BSSE is also reported. The ΔG values become monotonically more negative as the cage size grows up to C_{80}, when it stabilizes. The encapsulation becomes exergonic only from C_{70} on, with ΔG values around −30 kcal/mol.

As mentioned in the introduction, the most stable allotrope of phosphorous is the tetra atomic P_4.[7]

The electronic and Gibbs energy values for the formation of P_2 from P_4 (Scheme 2) according to our calculations are +32.8 and + 27.6 kcal/mol, respectively.

Thus, the encapsulation would be thermodynamically favored in the cases where the corresponding ΔG values are below −27.6 kcal/mol. As see in Table 2, $P_2@C_{70}$ already reaches this value. However, we estimate a BSSE on the encapsulation energy of around 2 kcal/mol, which would make the $P_2@C_{70}$ formation still endergonic. Nonetheless, in the case of the larger endohedrals the BSSE-corrected encapsulation Gibbs energies are negative enough to compensate for dissociation of P_4, thus making these species feasible from a thermodynamically point of view.

We have also considered the encapsulation of P_4 by the fullerenes, to yield the corresponding $P_4@C_n$ species. The electronic and Gibbs energies can be also found in the Table 2. Our calculations
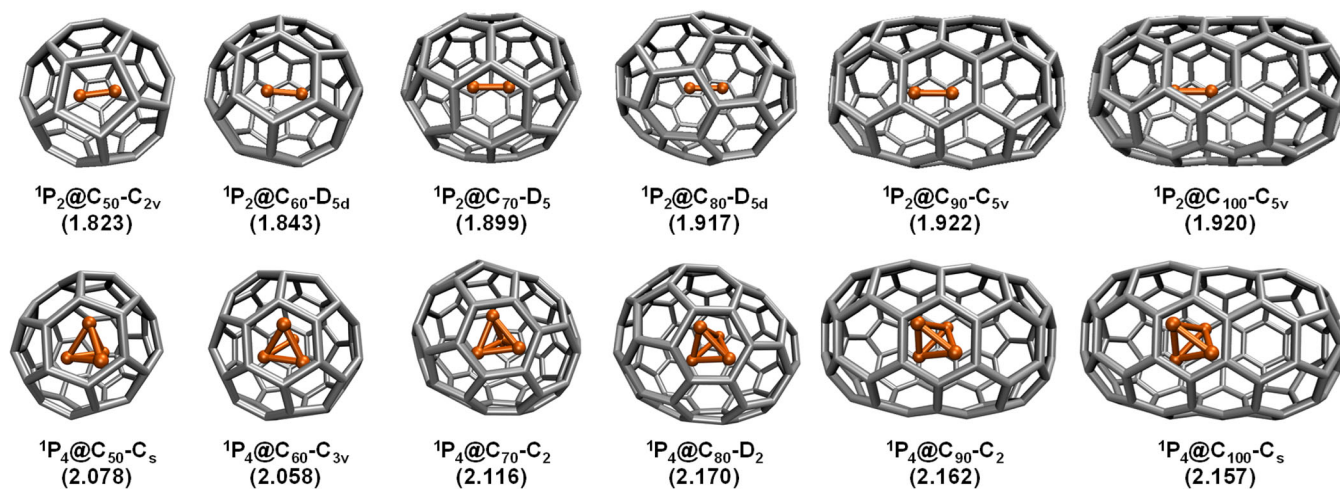
FIGURE 1 Optimized geometries of endohedrals $P_2@C_n$ and $P_4@C_n$ ($n = 50, 60, 70, 80, 90,$ and 100) at the BP86-D3(BJ)/def2-SVP level of theory. Symmetry of the endohedrals and average P–P bond length in [Å].

TABLE 2 Change of symmetry after P_2 or P_4 encapsulation, electronic energy (ΔE), Gibbs energy (ΔG) for the encapsulation of P_2 and P_4 by C_n ($n = 50, 60, 70, 80, 90,$ and 100), and basis set superposition error (BSSE) estimation.[a,b]

		P_2				P_4			
	Isomer	Symmetry	ΔE	BSSE	ΔG	Symmetry	ΔE	BSSE	ΔG
C_{50}	271	$D_{5h} \rightarrow C_{2v}$	87.1	2.9	96.1	$D_{5h} \rightarrow C_s$	418.9	7.1	421.8
C_{60}	1812	$I_h \rightarrow D_{5h}$	8.7	2.7	19.2	$I_h \rightarrow C_{3v}$	215.1	4.1	217.1
C_{70}	8149	$D_{5h} \rightarrow D_{5h}$	−40.0	2.3	−27.8	$D_{5h} \rightarrow C_2$	71.5	3.9	83.8
C_{80}	31,919	$D_2 \rightarrow D3_2$	−47.8	1.9	−36.4	$D_2 \rightarrow D_2$	−7.8	3.6	7.4
C_{90}	99,873	$D_{5h} \rightarrow C_{5v}$	−46.3	1.8	−35.0	$D_{5h} \rightarrow C_2$	40.3	3.2	52.8
C_{100}	285,464	$D_{5d} \rightarrow C_{5v}$	−44.7	1.8	−33.1	$D_{5d} \rightarrow C_s$	53.7	3.1	66.2

Note: The numbering of the isomers stems from lexicographically ordered face-spiral pentagon indices.
[a]All values are in in kcal/mol.
[b]All calculations have been performed at the BP86-D3(BJ)/def2-TZVP//BP86-D3(BJ)/def2-SVP level of theory.
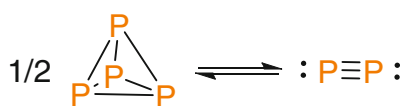
SCHEME 2 Dissociation of P_4.

suggest a highly endergonic process in all cases with values well over +50 kcal/mol, except for the case of C_{80} where the spherical shape helps a better fit of the P_4 inside the cage. Still, the overall formation of $P_4@C_{80}$ is not favored with respect to that of $P_2@C_{80}$.

We explored the possible relationship between the energetics of the encapsulation and geometrical parameters of the cages for $P_2@C_n$. Two parameters have been introduced to quantify the deformation of the C_n cages upon encapsulation. On the one hand, d_{max} is defined as the difference (in Å) between the maximum C–C distance of the endohedral species and that of the pristine cage. On the other hand, one can also consider, for each C atom of the cage, which is the furthest one. Averaging over all C atoms gives an average maximum distance (the corresponding standard deviation would measure its
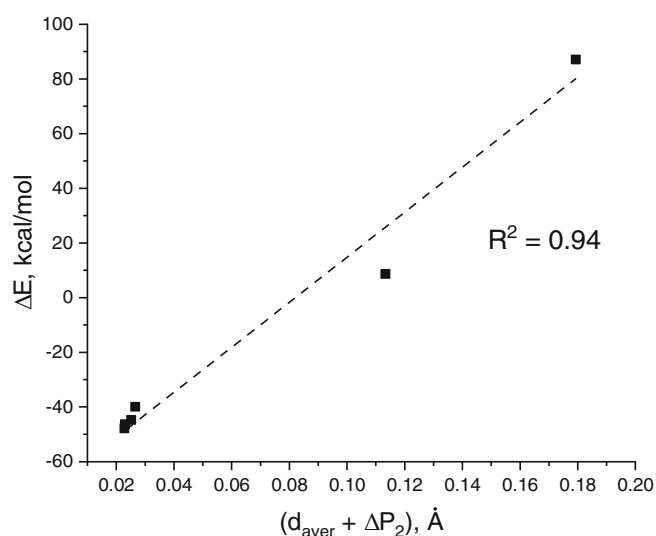

FIGURE 2 Encapsulation energy ΔE (kcal/mol) for the reaction $P_2@C_n$ ($n = 50, 60, 70, 80, 90,$ and 100) with respect to the total geometrical deformation of the host and guest ($d_{aver} + \Delta P_2$).

TABLE 3 P—P bond orders (BO, in a.u.) and partial charges (Q, in a.u.) of the P_2 and P_4 unit from Hilbert-space (NAO) and real-space (TFVC) analyses

Endohedral	WBO (NAO)	FBO (TFVC)	Q (NAO)	Q (TFVC)
P_2	3.00	3.08	0.00	0.00
$P_2@C_{50}$	2.71	2.09	0.19	0.60
$P_2@C_{60}$	2.92	2.43	−0.20	0.29
$P_2@C_{70}$	2.92	2.57	−0.04	0.26
$P_2@C_{80}$	2.92	2.62	−0.02	−0.26
$P_2@C_{90}$	2.89	2.58	−0.03	−0.26
$P_2@C_{100}$	2.88	2.57	−0.03	−0.27
P_4	1.01	1.18	0.00	0.00
$P_4@C_{50}$	0.83	0.78	0.52	2.46
$P_4@C_{60}$	0.99	0.97	−0.09	0.47
$P_4@C_{70}$	0.99	1.00	−0.06	0.46
$P_4@C_{80}$	0.99	1.01	−0.03	0.47
$P_4@C_{90}$	0.98	1.00	−0.02	0.50
$P_4@C_{100}$	0.98	1.00	−0.03	0.51

Note: All calculations have been performed at the BP86-D3(BJ)/def2-TZVP//BP86-D3(BJ)/def2-SVP level of theory.

spherical character). The parameter d_{aver} is defined as the difference of that average maximum C—C distance between the endohedral and the free cage. Thus, d_{max} and d_{aver} have positive values accounting for the cage deformation upon encapsulation. The change in P_2 bond length, ΔP_2, trivially accounts for the guest's deformation.

The values of d_{max} and d_{aver} are summarized in Table S2 of the Supporting Information. The encapsulation energies exhibit good correlation with the d_{aver} parameter, but not quite if one focuses on the larger cages where the d_{aver} values are much smaller than for C_{50} or C_{60}. Even worst correlation is found between the encapsulation energy and the P_2 deformation. However, the encapsulation energies do correlate very well with the total host-guest geometry deformation (defined as $d_{aver} + \Delta P_2$), as shown in Figure 2. The smaller the deformation, the better.

4 | BONDING ANALYSIS

4.1 | Frontier molecular orbitals

It is not easy to trace the origin of the deformation of each cage. However, that of the P_2 moiety should be related to the shape of the molecular orbitals in which the P_2 unit is primarily involved and the corresponding P—P bond order. In the free P_2 species, the σ and two π bonding orbitals are occupied, consistent with a formal triple bond. Charge transfer from the cage to the P_2 host would populate its antibonding orbitals, leading to a decrease of the bond order and a concomitant P—P stretch. Nevertheless, similarly, any charge transfer from the P_2 moiety to the cage would depopulate P—P bonding orbitals, causing the same effect. This means that the P—P bond order

can only decrease upon encapsulation, disregarding the P—P distance. A similar analysis involves P_4 unit, where the frontier orbitals consist of σ (e, t_2) and σ* (t_2) P—P orbitals.[70] Thus, the observed compression of the P—P bond upon encapsulation on the smaller cages is due to the steric pressure of the cage (this will be more evident from the EDA analysis below).

Table 3 gathers the P_2 and P_4 bond orders and partial charges obtained with a Hilbert-space (NAO) and a real-space (TFVC) atomic definitions. The large disagreement between different atomic population analysis in endohedral fullerenes has been pinpointed. For instance, in the endohedral borospherene complex $Cl@B_{39}$, the charge on Cl changes from −0.62 to 0.76 e depending on the method used.[71] In that work, the authors found that real-space QTAIM charges are reliable. We use here real-space TFVC charges because they provide similar results to QTAIM charges at much lower cost.

The TFVC method predicts a charge transfer from the P_2 moiety to the cage up to C_{70}, and the opposite effect from C_{80}. The charge transfer is very modest (ca. 0.3e) except for the smaller cage. On the other hand, NPA charges are usually negative for P_2, and much smaller. Such a charge flow is equally distributed over the entire cage (see Figure S3 in the ESI). As mentioned above, any charge transfer (positive or negative) should induce a decrease of the P—P bond order. This is exactly what is observed with both schemes. The predicted effect on the bond order is much more pronounced for the TFVC method, going down to 2.09 for the $P_2@C_{50}$ species, where the charge transfer is maximal. However, for the most interesting larger cages the bond order of the P—P bond remains similar to that of the free P_2 unit, indicating that upon encapsulation, the triple bond character of the P_2 host is maintained. Similarly, P_4 shows a significant charge transfer for the small cages, which is related to the reduction of the P—P bond order. With the size increase, charge transfer becomes smaller, and the bond order approaches the one observed for free P_4 molecule.

Molecular orbital analysis has been carried out focusing on the σ and π orbitals of the P_2 fragment at the BP86-D3(BJ)/def2-TZVP level of theory. As shown on Figure 3, the encapsulation induces an inversion of the relative energies of the σ and π orbital of P_2. Thus, while for free P_2 the σ is lower in energy, the contrary is found upon encapsulation for the smaller cages C_{50} and C_{60}. This is likely to be due to the increased Pauli repulsion suffered by the σ electrons that are closer to the cage than the π ones. Also, in the smaller cages (C_{50}, C_{60}), the σ and π orbital of P_2 orbitals are energetically destabilized for the same reason. In fact, in both cases the σ orbital becomes the HOMO−1. Then, the larger the cage, the more stabilized the σ and π orbitals become. The contrary occurs for the σ* and π* ones (not shown). It is also worth to note that the degeneracy of the π and π* orbitals is lost in the case of $P_2@C_{50}$ and $P_2@C_{80}$.

4.2 | Energy decomposition analysis

More detailed information about the nature of the interaction between P_2 and C_n (n = 50, 60, 70, 80, 90, and 100) fullerene cages
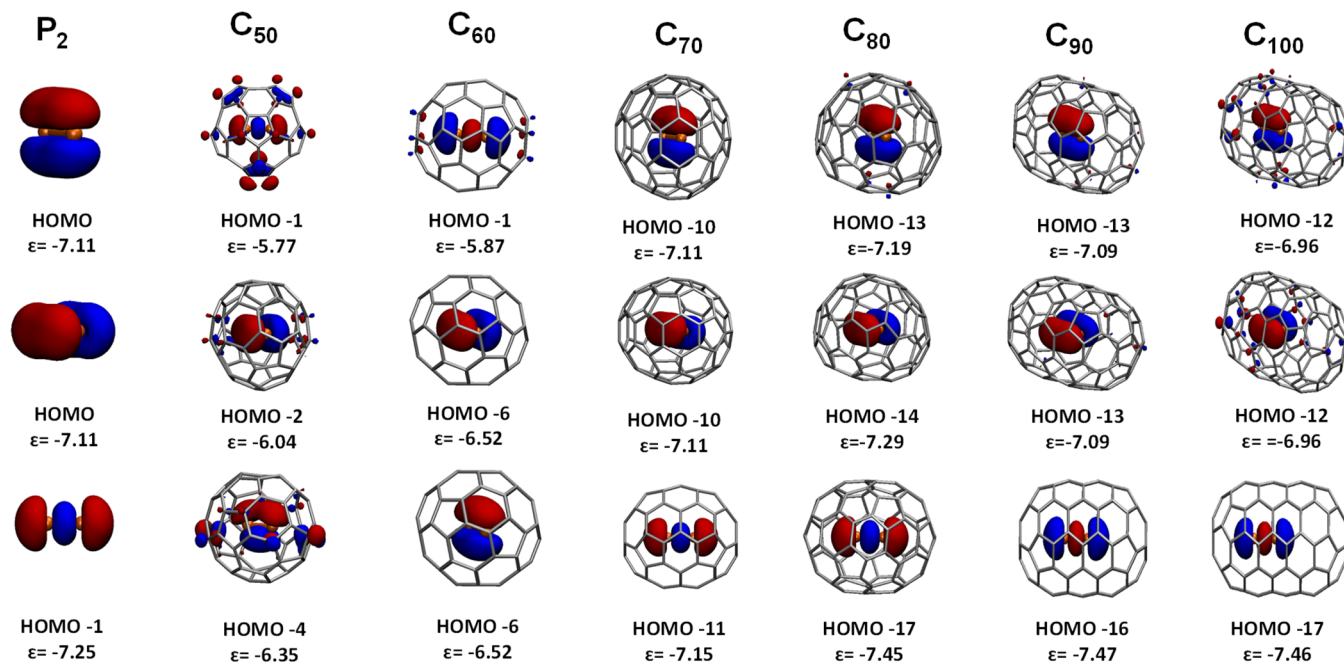
FIGURE 3   Molecular orbitals (isovalue = 0.04) with σ and π symmetry for $P_2@C_n$ (n = 50, 60,70, 80, 90, and 100) with their energies in eV at the BP86-D3(BJ)/def2-TZVP//BP86-D3(BJ)/def2-SVP level of theory.

TABLE 4   Energy decomposition analysis for the interaction between the P_2/P_4 and C_n (n = 50, 60,70, 80, 90, and 100) at the BP86-D3(BJ)/TZ2P//BP86-D3(BJ)/def2-SVP level of theory

	$P_2@C_{50}$[a]	$P_2@C_{60}$	$P_2@C_{70}$	$P_2@C_{80}$	$P_2@C_{90}$	$P_2@C_{100}$
ΔE_{int}	65.6	2.6	−39.9	−47.1	−44.5	−42.6
ΔE_{Pauli}	437.2	220.0	90.4	54.7	53.1	57.6
ΔE_{elst}[b]	−223.3 (60.1%)	−116.2 (53.5%)	−50.9 (39.1%)	−31.1 (30.5%)	−28.7 (29.4%)	−30.7 (30.7%)
ΔE_{disp}[b]	−43.7 (11.7%)	−56.1 (25.8%)	−60.5 (46.4%)	−57.9 (56.8%)	−56.1 (57.5%)	−55.6 (55.5%)
ΔE_{orb}[b]	−104.6 (28.2%)	−45.1 (20.7%)	−18.9 (14.5%)	−12.9 (12.7%)	−12.8 (13.1%)	−13.9 (13.8%)
ΔE_{prep}	25.4	9.0	1.7	0.0	0.0	0.0
D_e	−91.0	−11.6	38.2	47.1	44.5	42.6
	$P_4@C_{50}$	$P_4@C_{60}$	$P_4@C_{70}$	$P_4@C_{80}$	$P_4@C_{90}$	$P_4@C_{100}$
ΔE_{int}	311.8	153.3	37.6	−27.6	13.8	22.7
ΔE_{Pauli}	1902.5	735.6	440.6	272.7	339.0	356.0
ΔE_{elst}[b]	−863.1 (54.3%)	−358.1 (64.6%)	−221.4 (54.9%)	−147.8 (49.2%)	−166.0 (51.0%)	−174.2 (52.3%)
ΔE_{disp}[b]	−64.8 (4.1%)	−56.1 (10.1%)	−94.1 (23.3%)	−96.4 (32.1%)	−89.2 (27.4%)	−87.1 (26.1%)
ΔE_{orb}[b]	−662.7 (41.7%)	−140.6 (25.3%)	−87.5 (21.7%)	−56.1 (18.7%)	−70.0 (21.5%)	−72.0 (21.6%)
ΔE_{prep}	114.5	65.6	36.9	21.1	28.8	33.4
D_e	−426.4	−218.9	−74.5	6.5	−42.5	−56.0

[a]All energy values are given in kcal/mol.
[b]The value in parenthesis gives the percentage contribution to the total attractive interactions $\Delta E_{elst} + \Delta E_{orb} + \Delta E_{disp}$.

are provided by the results of the EDA method.[72] EDA has proven to be a useful tool to assess the nature of the chemical bond in main group compounds and transition metal compounds,[73] as well as the interaction in endohedrals.[74] Nonetheless, a recent discussion has been placed about the path function nature of the energy components.[75] Within EDA scheme, the interaction formation between two

(or more) fragments is divided into Pauli repulsion, electrostatic interaction, and orbital interaction (for further details, see the computational section).

Table 4 shows the numerical results of the calculations where P_2 and C_n (n = 50, 60, 70, 80, 90, and 100) are both in singlet reference state in each fragment (see also Table S1). Thus, the P_2 species keeps

the triple bond and the two lone pairs intact, according to the Frontier Molecular Orbitals displayed in Figure 3. The interaction energies ΔE_{int} follows the same trend as the dissociation energy (D_e) for the bigger fullerenes (from n = 70 to 100). For those cases, the preparation of the fragments (ΔE_{prep}) does not carry particular energy penalties as there is no significant deformation of the P_2 molecule or the fullerene cage upon complexation. This observation is in good agreement with the deformation analysis discussed above. Note, however, that this dissociation energy is negative for the C_{50} and C_{60} fullerenes and the preparation energy is not negligible, that is, 25.4 and 9.0 kcal/mol, respectively.

ΔE_{int} is positive for C_{50} (+65.6 kcal/mol) and decreases with the size of the cage until C_{100} (−42.6 kcal/mol). The dissection of the ΔE_{int} reveals that the Pauli repulsion is a strongly destabilizing factor for smaller fullerenes cages, as there is not enough space for hosting the P_2 molecule. As the size increases, the sum of the stabilizing interactions overcome the repulsive interaction. Interestingly, the dispersion interaction dominates the stabilization for C_{70} (46.4%), C_{80} (56.8%), C_{90} (57.5%), and C_{100} (55.5%). This observation is in good agreement with other reported systems.[76] The second stabilizing contribution comes from the electrostatic interaction counting for 30%–40% for the stable encapsulations. The orbital interaction contributes with about ∼10% for the attractive interaction and it becomes bigger for the smaller cages, namely 28.2% for C_{50} and 20.7% for C_{60}. This small contribution of the orbital interaction term is in line with the partial charges computed in Table 4, revealing a small charge transfer from P_2 to the fullerenes.

Table 4 also gathers the EDA results for the encapsulation of P_4 with C_n (n = 50, 60, 70, 80, 90, and 100) in the singlet reference state. As discussed above, this process is thermodynamically unfavorable for all cases, resulting in negative dissociation energy values. The only exception is C_{80}, where the internal space is enough to host P_4 with a slightly positive D_e value of 6.5 kcal/mol. Nonetheless, bigger cages C_{90} and C_{100} yield negative D_e values as a consequence of the spheroidal shape. The preparation energy values (ΔE_{prep}) suggest high energy penalties upon complexation, going from 114.5 kcal/mol (C_{50}) to 21.1 kcal/mol (C_{80}). In addition, the interaction energy values (ΔE_{int}) reveal a destabilizing effect by the encapsulation caused by strong Pauli repulsion between the host and the guest.

5 | CONCLUSIONS

The feasibility of the encapsulation of P_2 in C_n fullerenes has been computationally assessed for cages from n = 50 to n = 100. We show fullerenes C_{70} to C_{100} are suitable cages to incorporate P_2 instead of P_4, which is the most stable form of phosphorous. Upon inclusion of thermal and entropic effects, only the formation of endohedral C_{80} to C_{100} overcome the energetic penalty for the required P_4 dissociation into two P_2 dimers. Orbital analysis indicates that the triple bond in P_2 remains intact within the endohedral system, with very small host-guest charge-transfer. EDA shows that Pauli repulsion is roughly twice the amount of the (favorable) electrostatic interaction along the series.

The dispersion energy contribution amounts to ca. −55 to −60 kcal/mol for all cages except the smallest one. From n = 70 on, the dispersion becomes dominant and accounts for the favorable encapsulation energies of P_2 in C_{70} to C_{100} cages.

DATA AVAILABILITY STATEMENT

Data available in article supplementary material.

ORCID

Enric Sabater https://orcid.org/0000-0002-2879-7627
Miquel Solà https://orcid.org/0000-0002-1917-7450
Diego M. Andrada https://orcid.org/0000-0003-2515-7859

REFERENCES

[1] (a) P. P. Power, *Chem. Rev.* **1999**, *99*, 3463. (b) R. C. Fischer, P. P. Power, *Chem. Rev.* **2010**, *110*, 3877.
[2] P. Jutzi, *Angew. Chem., Int. Ed.* **1975**, *14*, 232.
[3] (a) D. J. Liptrot, P. P. Power, *Nat. Rev. Chem.* **2017**, *1*, 1. (b) J. P. Wagner, P. R. Schreiner, *Angew. Chem., Int. Ed.* **2015**, *54*, 12274.
[4] V. Nesterov, D. Reiter, P. Bag, P. Frisch, R. Holzner, A. Porzelt, S. Inoue, *Chem. Rev.* **2018**, *118*, 9678.
[5] N. N. Greenwood, A. Earnshaw, *Chemistry of the Elements*, Elsevier, Oxford **2012**.
[6] D. E. Canfield, A. N. Glazer, P. G. Falkowski, *Science* **2010**, *330*, 192.
[7] F. Bachhuber, J. von Appen, R. Dronskowski, P. Schmidt, T. Nilges, A. Pfitzner, R. Weihrich, *Angew. Chem., Int. Ed.* **2014**, *53*, 11629.
[8] H. Bock, H. Mueller, *Inorg. Chem.* **1984**, *23*, 4365.
[9] A. Kornath, A. Kaufmann, M. Torheyden, *J. Chem. Phys.* **2002**, *116*, 3323.
[10] S. G. Lias, J. E. Bartmess, J. F. Liebman, J. L. Holmes, R. D. Levin, W. G. Mallard, *J. Phys. Chem. Ref. Data* **1988**, *17*, 1.
[11] R. S. Mulliken, B. Liu, *J. Am. Chem. Soc.* **1971**, *93*, 6738.
[12] W. Kutzelnigg, *Angew. Chem., Int. Ed.* **1984**, *23*, 272.
[13] P. Jerabek, G. Frenking, *Theo. Chem. Acc.* **2014**, *133*, 1447.
[14] J. S. Figueroa, C. C. Cummins, *Dalton Trans.* **2006**, 2161.
[15] J. Borm, G. Huttner, O. Orama, L. Zsolnai, *J. Organomet. Chem.* **1985**, *282*, 53.
[16] (a) B. M. Cossairt, N. A. Piro, C. C. Cummins, *Chem. Rev.* **2010**, *110*, 4164. (b) M. Caporali, L. Gonsalvi, A. Rossin, M. Peruzzini, *Chem. Rev.* **2010**, *110*, 4178. (c) M. Scheer, G. Balázs, A. Seitz, *Chem. Rev.* **2010**, *110*, 4236.
[17] (a) H. Schafer, D. Binder, D. Fenske, *Angew. Chem., Int. Ed.* **1985**, *24*, 522. (b) O. J. Scherer, M. Ehses, G. Wolmershäuser, *Angew. Chem.,*

Int. Ed. **1998**, *37*, 507. (c) B. Zarzycki, T. Zell, D. Schmidt, U. Radius, *Eur. J. Inorg. Chem.* **2013**, *2013*, 2051. (d) S. L. Yao, N. Lindenmaier, Y. Xiong, S. Inoue, T. Szilvasi, M. Adelhardt, J. Sutter, K. Meyer, M. Driess, *Angew. Chem., Int. Ed.* **2015**, *54*, 1250. (e) S. L. Yao, T. Szilvasi, N. Lindenmaier, Y. Xiong, S. Inoue, M. Adelhardt, J. Sutter, K. Meyer, M. Driess, *Chem. Comm.* **2015**, *51*, 6153. (f) L. N. Grant, B. Pinter, B. C. Manor, R. Suter, H. Grutzmacher, D. J. Mindiola, *Chem. – Eur. J.* **2017**, *23*, 6272. (g) J. Du, D. Hunger, J. A. Seed, J. D. Cryer, D. M. King, A. J. Wooles, J. van Slageren, S. T. Liddle, *J. Am. Chem. Soc.* **2021**, *143*, 5343.

[18] N. A. Piro, J. S. Figueroa, J. T. McKellar, C. C. Cummins, *Science* **2006**, *313*, 1276.

[19] (a) E. B. Hulley, P. T. Wolczanski, E. B. Lobkovsky, *Chem. Comm.* **2009**, 6412. (b) L. Liu, D. A. Ruiz, F. Dahcheh, G. Bertrand, R. Suter, A. M. Tondreau, H. Grutzmacher, *Chem. Sci.* **2016**, *7*, 2335.

[20] C. Esterhuysen, G. Frenking, *Chem. – Eur. J.* **2003**, *9*, 3518.

[21] J. Sun, H. Verplancke, J. I. Schweizer, M. Diefenbach, C. Wurtele, M. Otte, I. Tkach, C. Herwig, C. Limberg, S. Demeshko, M. C. Holthausen, S. Schneider, *Chem* **2021**, *7*, 1952.

[22] Y. Wang, Y. Xie, P. Wei, R. B. King, H. F. Schaefer, P. V. R. Schleyer, G. H. Robinson, *J. Am. Chem. Soc.* **2008**, *130*, 14970.

[23] (a) O. Back, G. Kuchenbeiser, B. Donnadieu, G. Bertrand, *Angew. Chem., Int. Ed.* **2009**, *48*, 5530. (b) O. Back, B. Donnadieu, P. Parameswaran, G. Frenking, G. Bertrand, *Nat. Chem.* **2010**, *2*, 369.

[24] (a) S.-S. Asami, M. Okamoto, K. Suzuki, M. Yamashita, *Angew. Chem., Int. Ed.* **2016**, *55*, 12827. (b) D. W. N. Wilson, M. P. Franco, W. K. Myers, J. E. McGrady, J. M. Goicoechea, *Chem. Sci.* **2020**, *11*, 862.

[25] Y. Wang, T. Szilvási, S. Yao, M. Driess, *Nat. Chem.* **2020**, *12*, 801.

[26] N. Holzmann, G. Frenking, *Z. Naturforsch. A.* **2014**, *69*, 385–395.

[27] A. A. Popov, S. Yang, L. Dunsch, *Chem. Rev.* **2013**, *113*, 5989.

[28] J. R. Heath, S. C. O'Brien, Q. Zhang, Y. Liu, R. F. Curl, F. K. Tittel, R. E. Smalley, *J. Am. Chem. Soc.* **1985**, *107*, 7779.

[29] (a) K. A. Caldwell, D. E. Giblin, C. S. Hsu, D. Cox, M. L. Gross, *J. Am. Chem. Soc.* **1991**, *113*, 8519. (b) T. Weiske, D. K. Böhme, J. Hrušák, W. Krätschmer, H. Schwarz, *Angew. Chem. Int. Ed. Eng.* **1991**, *30*, 884. (c) D. E. Giblin, M. L. Gross, M. Saunders, H. Jimenez-Vazquez, R. J. Cross, *J. Am. Chem. Soc.* **1997**, *119*, 9883.

[30] (a) Y. Kubozono, H. Maeda, Y. Takabayashi, K. Hiraoka, T. Nakai, S. Kashino, S. Emura, S. Ukita, T. Sogabe, *J. Am. Chem. Soc.* **1996**, *118*, 6998. (b) J. Ding, S. Yang, *J. Am. Chem. Soc.* **1996**, *118*, 11254. (c) K. Kobayashi, S. Nagase, M. Yoshida, E. Ōsawa, *J. Am. Chem. Soc.* **1997**, *119*, 12693. (d) H. Okada, T. Komuro, T. Sakai, Y. Matsuo, Y. Ono, K. Omote, K. Yokoo, K. Kawachi, Y. Kasama, S. Ono, R. Hatakeyama, T. Kaneko, H. Tobita, *RSC Adv.* **2012**, *2*, 10624.

[31] (a) M. N. Chaur, F. Melin, A. L. Ortiz, L. Echegoyen, *Angew. Chem., Int. Ed.* **2009**, *48*, 7514. (b) X. Zhang, Y. Wang, R. Morales-Martínez, J. Zhong, C. de Graaf, A. Rodríguez-Fortea, J. M. Poblet, L. Echegoyen, L. Feng, N. Chen, *J. Am. Chem. Soc.* **2018**, *140*, 3907. (c) C. Foroutan-Nejad, J. Vícha, R. Marek, M. Patzschke, M. Straka, *Phys. Chem. Chem. Phys.* **2015**, *17*, 24182. (d) A. Jaroš, C. Foroutan-Nejad, M. Straka, *Inorg. Chem.* **2020**, *59*, 12608.

[32] R. Valencia, A. Rodríguez-Fortea, A. Clotet, C. de Graaf, M. N. Chaur, L. Echegoyen, J. M. Poblet, *Chem. – Eur. J.* **2009**, *15*, 10997.

[33] K. Komatsu, M. Murata, Y. Murata, *Science* **2005**, *307*, 238.

[34] (a) K. Kurotobi, Y. Murata, *Science* **2011**, *333*, 613. (b) E. E. Maroto, J. Mateos, M. Garcia-Borràs, S. Osuna, S. Filippone, M. Á. Herranz, Y. Murata, M. Solà, N. Martín, *J. Am. Chem. Soc.* **2015**, *137*, 1190.

[35] S.-I. Iwamatsu, C. M. Stanisky, R. J. Cross, M. Saunders, N. Mizorogi, S. Nagase, S. Murata, *Angew. Chem., Int. Ed.* **2006**, *45*, 5337.

[36] (a) A. Krachmalnicoff, R. Bounds, S. Mamone, M. H. Levitt, M. Carravetta, R. J. Whitby, *Chem. Comm.* **2015**, *51*, 4993. (b) S. Vidal, M. Izquierdo, S. Alom, M. Garcia-Borràs, S. Filippone, S. Osuna, M. Solà, R. J. Whitby, N. Martín, *Chem. Comm.* **2017**, *53*, 10993.

[37] S. Bloodworth, G. Sitinova, S. Alom, S. Vidal, G. R. Bacanu, S. J. Elliott, M. E. Light, J. M. Herniman, G. J. Langley, M. H. Levitt, R. J. Whitby, *Angew. Chem., Int. Ed.* **2019**, *58*, 5038.

[38] K. E. Whitener, M. Frunzi, S.-I. Iwamatsu, S. Murata, R. J. Cross, M. Saunders, *J. Am. Chem. Soc.* **2008**, *130*, 13996.

[39] T. Futagoishi, M. Murata, A. Wakamiya, Y. Murata, *Angew. Chem., Int. Ed.* **2015**, *54*, 14791.

[40] Y. Li, N. Lou, D. Xu, C. Pan, X. Lu, L. Gan, *Angew. Chem., Int. Ed.* **2018**, *57*, 14144.

[41] M. Murata, Y. Murata, K. Komatsu, *Chem. Comm.* **2008**, 6083.

[42] (a) M. Murata, S. Maeda, Y. Morinaka, Y. Murata, K. Komatsu, *J. Am. Chem. Soc.* **2008**, *130*, 15800. (b) Y. Murata, S. Maeda, M. Murata, K. Komatsu, *J. Am. Chem. Soc.* **2008**, *130*, 6702. (c) N. J. Turro, A. A. Marti, J. Y. C. Chen, S. Jockusch, R. G. Lawler, M. Ruzzi, E. Sartori, S. C. Chuang, K. Komatsu, Y. Murata, *J. Am. Chem. Soc.* **2008**, *130*, 10506.

[43] (a) S. Jalife, J. Arcudia, S. Pan, G. Merino, *Chem. Sci.* **2020**, *11*, 6642. (b) S. Jalife, S. Mondal, J. L. Cabellos, S. Pan, M. Á. Méndez-Rojas, I. Fernández, G. Frenking, G. Merino, *ChemistrySelect* **2016**, *1*, 2405. (c) M. Garcia-Borràs, S. Osuna, M. Swart, J. M. Luis, M. Solà, *Angew. Chem., Int. Ed.* **2013**, *52*, 9275. (d) A. Rodríguez-Fortea, N. Alegret, A. L. Balch, J. M. Poblet, *Nat. Chem.* **2010**, *2*, 955. (e) Y. Wang, S. Díaz-Tendero, F. Martín, M. Alcamí, *J. Am. Chem. Soc.* **2016**, *138*, 1551.

[44] M. Mantina, A. C. Chamberlin, R. Valero, C. J. Cramer, D. G. Truhlar, *J. Phys. Chem. A* **2009**, *113*, 5806.

[45] (a) K. P. Huber, G. Herzberg, *Molecular Spectra and Molecular Structure: IV*, Springer US, Constants of Diatomic Molecules **1979**, p. 8. (b) N. J. Brassington, H. G. M. Edwards, D. A. Long, *J. Raman. Spectrosc.* **1981**, *11*, 346.

[46] L. C. Ducati, N. Takagi, G. Frenking, *J. Chem. Phys. A* **2009**, *113*, 11693.

[47] M. J. Frisch, G. W. Trucks, H. B. Schlegel, G. E. Scuseria, M. A. Robb, J. R. Cheeseman, G. Scalmani, V. Barone, G. A. Petersson, H. Nakatsuji, X. Li, M. Caricato, A. V. Marenich, J. Bloino, B. G. Janesko, R. Gomperts, B. Mennucci, H. P. Hratchian, J. V. Ortiz, A. F. Izmaylov, J. L. Sonnenberg, D. Williams-Young, F. Ding, F. Lipparini, F. Egidi, J. Goings, B. Peng, A. Petrone, T. Henderson, D. Ranasinghe, V. G. Zakrzewski, J. Gao, N. Rega, G. Zheng, W. Liang, M. Hada, M. Ehara, K. Toyota, R. Fukuda, J. Hasegawa, M. Ishida, T. Nakajima, Y. Honda, O. Kitao, H. Nakai, T. Vreven, K. Throssell, J. J. A. Montgomery, J. E. Peralta, F. Ogliaro, M. J. Bearpark, J. J. Heyd, E. N. Brothers, K. N. Kudin, V. N. Staroverov, T. A. Keith, R. Kobayashi, J. Normand, K. Raghavachari, A. P. Rendell, J. C. Burant, S. S. Iyengar, J. Tomasi, M. Cossi, J. M. Millam, M. Klene, C. Adamo, R. Cammi, J. W. Ochterski, R. L. Martin, K. Morokuma, O. Farkas, J. B. Foresman, D. J. Fox, Gaussian 16, Revision C.01. Gaussian, Inc., Wallingford CT **2019**.

[48] P. Schwerdtfeger, L. Wirz, J. Avery, *J. Comput. Chem.* **2013**, *34*, 1508.

[49] P. W. Fowler, D. E. Manolopoulos, *An Atlas of Fullerenes*, Dover Publications, Mineola, New York **2006**.

[50] C. Y. Peng, P. Y. Ayala, H. B. Schlegel, M. J. Frisch, *J. Comput. Chem.* **1996**, *17*, 49.

[51] (a) A. D. Becke, E. R. Johnson, *J. Chem. Phys.* **2005**, *123*, 154101. (b) S. Grimme, S. Ehrlich, L. Goerigk, *J. Comput. Chem.* **2011**, *32*, 1456. (c) E. R. Johnson, A. D. Becke, *J. Chem. Phys.* **2005**, *123*, 24101.

[52] A. E. Reed, R. B. Weinstock, F. Weinhold, *J. Chem. Phys.* **1985**, *83*, 735.

[53] E. D. Glendening, J. K. Badenhoop, A. E. Reed, J. E. Carpenter, J. A. Bohmann, C. M. Morales, P. Karafiloglou, C. R. Landis, F. Weinhold, *GENNBO 7.0*, Theoretical Chemistry Institute, University of Wisconsin, Madison **2018**.

[54] P. Salvador, E. Ramos-Córdoba, *J. Chem. Phys.* **2013**, *139*, 71103.

[55] P. Salvador, E. Ramos-Córdoba, M. Gimferrer, *Universitat de Girona*, Girona **2020**.

[56] K. Morokuma, *J. Chem. Phys.* **1971**, *55*, 1236.

[57] (a) T. Ziegler, A. Rauk, *Inorg. Chem.* **1979**, *18*, 1558. (b) T. Ziegler, A. Rauk, *Inorg. Chem.* **1979**, *18*, 1755.

[58] J. Krijn, E. J. Baerends, *Fit Func. HFS-Method*, **1984**.

[59] E. Van Lenthe, E. J. Baerends, J. G. Snijders, *J. Chem. Phys.* **1993**, *99*, 4597.

[60] F. M. Bickelhaupt, N. M. M. Nibbering, E. M. Van Wezenbeek, E. J. Baerends, *J. Phys. Chem.* **1992**, *96*, 4864.

[61] S. Grimme, J. Antony, S. Ehrlich, H. Krieg, *J. Chem. Phys.* **2010**, *132*, 132.

[62] (a) F. M. Bickelhaupt, E. J. Baerends, in *Reviews in computational chemistry*, Vol. 15 (Eds: K. B. Lipkowitz, D. B. Boyd). Wiley, Weinheim **2000**, p. 1. (b) G. te Velde, F. M. Bickelhaupt, E. J. Baerends, C. Fonseca Guerra, S. J. A. van Gisbergen, J. G. Snijders, T. Ziegler, *J. Comput. Chem.* **2001**, *22*, 931.

[63] H. Kroto, *Nature* **1987**, *329*, 529.

[64] H. Ajie, M. M. Alvarez, S. J. Anz, R. D. Beck, F. Diederich, K. Fostiropoulos, D. R. Huffman, W. Kraetschmer, Y. Rubin, et al, *J. Phys. Chem.* **1990**, *94*, 8630.

[65] X. Zhao, *J. Phys. Chem. B* **2005**, *109*, 5267.

[66] F. H. Hennrich, R. H. Michel, A. Fischer, S. Richard-Schneider, S. Gilb, M. M. Kappes, D. Fuchs, K. Kobayashi, S. Nagase, *Angew. Chem., Int. Ed.* **1996**, *35*, 1732.

[67] R. Sure, A. Hansen, P. Schwerdtfeger, S. Grimme, *Phys. Chem. Chem. Phys.* **2017**, *19*, 14296.

[68] R. M. Koenig, H.-R. Tian, T. L. Seeler, K. R. Tepper, H. M. Franklin, Z.-C. Chen, S.-Y. Xie, S. Stevenson, *J. Am. Chem. Soc.* **2020**, *142*, 15614.

[69] T. G. Schmalz, W. A. Seitz, D. J. Klein, G. E. Hite, *J. Am. Chem. Soc.* **1988**, *110*, 1113.

[70] S. Evans, P. J. Joachim, A. F. Orchard, D. W. Turner, *Int. J. Mass Spectrom.* **1972**, *9*, 41.

[71] A. J. Stasyuk, M. Solà, A. A. Voityuk, *Sci. Rep.* **2018**, *8*, 2882.

[72] L. L. Zhao, M. von Hopffgarten, D. M. Andrada, G. Frenking, *WIREs Comput. Mol. Sci.* **2018**, *8*, e13450.

[73] (a) T. Sergeieva, D. Mandal, D. M. Andrada, *Chem. – Eur. J.* **2021**, *27*, 10601. (b) S. Danés, C. Muller, L. Wirtz, V. Huch, T. Block, R. Pottgen, A. Schäfer, D. M. Andrada, *Organometallics* **2020**, *39*, 516. (c) M. K. Sharma, D. Rottschäfer, B. Neumann, H. G. Stammler, S. Danés, D. M. Andrada, M. van Gastel, A. Hinz, R. S. Ghadwal, *Chem. – Eur. J.* **2021**, *27*, 5803. (d) G. Frenking, I. Fernández, N. Holzmann, S. Pan, I. Krossing, M. F. Zhou, *JACS Au* **2021**, *1*, 623.

[74] C. Foroutan-Nejad, M. Straka, I. Fernández, G. Frenking, *Angew. Chem., Int. Ed.* **2018**, *57*, 13931.

[75] (a) D. M. Andrada, C. Foroutan-Nejad, *Phys. Chem. Chem. Phys.* **2020**, *22*, 22459. (b) A. Krapp, G. Frenking, *Chem. – Eur. J.* **2007**, *13*, 8256. (c) J. Poater, D. M. Andrada, M. Solà, C. Foroutan-Nejad, *Phys. Chem. Chem. Phys.* **2022**, *24*, 2344. (d) M. Solà, M. Duran, J. Poater, *Theor. Chem. Acc.* **2021**, *140*, 33.

[76] R. Sure, R. Tonner, P. Schwerdtfeger, *J. Comput. Chem.* **2015**, *36*, 88.

SUPPORTING INFORMATION

Additional supporting information may be found in the online version of the article at the publisher's website.